Published in final edited form as:
J Am Soc Echocardiogr. 2010 January ; 23(1): 79. doi:10.1016/j.echo.2009.09.025.

Effect of Acoustic Power on *In Vivo* Molecular Imaging with Targeted Microbubbles: Implications for Low-Mechanical Index Real-Time Imaging

Beat A. Kaufmann, MD, **Chad L. Carr, MD**, **Todd Belcik, BS, RDCS, FASE**, **Aris Xie, MS**, **Benjamin Kron, BS**, **Qi Yue, MD**, and **Jonathan R. Lindner, MD, FASE**
Cardiovascular Division of Oregon Health & Science University; Portland, Oregon

Abstract

The aim of this study was to evaluate the influence of acoustic power on ultrasound molecular imaging data with targeted microbubbles. Imaging was performed with a contrast-specific multipulse method at a mechanical index (MI) of 0.18 and 0.97. *In vitro* imaging was used to measure concentration-intensity relationships and to assess whether damping from microbubble attachment to cultured endothelial cells affects signal enhancement. Power-related differences in signal enhancement were evaluated *in vivo* by P-selectin-targeted and control microbubble imaging in a murine model of hindlimb ischemia-reperfusion injury. During *in vitro* experiments there was minimal acoustic damping from microbubble-cell attachment at either MI. Signal enhancement in the *in vitro* and *in vivo* experiments was 2-3-fold higher for high-MI compared with low-MI imaging which was due to greater pixel intensity, detection of a greater number of retained microbubbles, and increased point-spread function. Yet, there was a linear relationship between high- and low-MI data indicating that the relative degree of enhancement was similar. We conclude that during molecular imaging high-MI protocols produce more robust targeted signal enhancement than low-MI, although differences in relative enhancement caused by condition or agent are similar.

Molecular imaging with contrast enhanced ultrasound relies on the detection of microbubbles or nanoparticles that are targeted to disease-specific molecules.1 In general, targeted agents are administered as a bolus and are then imaged by high-mechanical index (MI) ultrasound after a 5-10 min pause to allow clearance of freely-circulating microbubbles from the blood pool.2 Signal from targeted microbubbles is encoded in the first frame obtained upon resumption of imaging, after which signal decays from acoustic disruption of the agent.2,3 High-MI imaging has been used in most molecular imaging studies in order to maximize sensitivity for retained tracer. However, there has been increasing interest in using low-MI imaging in order to: (1) take advantage of frame averaging, (2) choose appropriate frames void of motion artifact from multipulse contrast techniques, and (3) facilitate 3-dimensional volume scanning. Also, real-time imaging will greatly improve the ease of localizing the tissue of interest which is important for transitioning ultrasound molecular imaging from anesthetized animals where the subject and probes are fixed to awake humans.

An important consideration when using low-MI imaging is whether signal enhancement will be sufficiently robust to evaluate subtle differences in molecular expression profile. Volumetric vibration of microbubbles in an acoustic field is substantially influenced by viscous and thermal damping from its microenvironment.[4-6] Microbubble attachment to biosurfaces may

Address correspondence to: Jonathan R. Lindner, MD, Cardiovascular Division, UHN-62, Oregon Health & Science University, 3181 SW Sam Jackson Park Rd., Portland, OR 97239, Telephone: (503) 494-8750, Fax: (503) 494-8550, lindnerj@ohsu.edu.

disproportionately affect non-linear signal generation when imaging at low-MI. This notion is supported by the finding that ultrasound frequency and/or amplitude response is altered when microbubbles are attached to particles, cells in suspension or cell monolayers.[7,8] The purpose of this study was to determine whether differences in targeted microbubble signal enhancement during high-MI and low-MI imaging *in vivo* influences molecular imaging data on expression profile.

Methods

Microbubble Preparation

Lipid-shelled decafluorobutane microbubbles were prepared by sonication of a gas-saturated aqueous suspension of distearoylphosphatidylcholine (2 mg/mL) and polyoxyethylene-40-stearate (1 mg/mL). For preparation of targeted microbubbles, distearoylphosphatidylethanolamine-PEG(2000)biotin (0.1 mg/mL) was added to the aqeuous suspension. Targeting ligands were conjugated to the microbubble surface using a biotin-streptavidin link as previously described.[2] Microbubbles were targeted to VCAM-1 or P-selectin by conjugation of rat anti-mouse IgG1 monoclonal antibody from hybridoma (clone MK2.7 for VCAM-1, RB40.34 for P-selectin). Control microbubbles were prepared in a similar fashion with isotype control antibody (R3-34, Pharmingen Inc, San Diego, CA). Microbubble size distribution and concentration were measured by electrozone sensing (Multisizer III, Beckman Coulter, Fullerton, CA).

Contrast Ultrasound

Ultrasound imaging *in vitro* and *in vivo* was performed with a linear array transducer (15L8) interfaced with a Sequoia ultrasound system (Siemens Medical Systems, Mountain View, CA). A multipulse algorithm using phase- and amplitude-modulation (Contrast Pulse Sequencing) was used to detect the non-linear fundamental component of the microbubble signal. Imaging was performed at 7 MHz with low-MI (0.18) and high-MI (0.97) settings. The dynamic range was set at 55dB and gain settings for each MI were adjusted at the beginning of each study to a level just below that which produced visible background speckle. Digital data were transferred to an off-line computer for analysis. Intensity on each imaging frame was transformed from a logarithmic to a linear scale using known dynamic range and span of intensity values. To ensure that the relationship between microbubble concentration and signal intensity at 7MHz was linear with low- and high-MI settings, concentration versus intensity plots were generated by imaging microbubbles suspended in a water bath.

Signal from Microbubble-Cell Complexes *in vitro*

Microbubble ligation to cultured endothelial cells was used as an *in vitro* model to determine the relative effect of attachment on signal intensity during high- and low-MI imaging. Murine endothelial cells (SVEC4-10, ATCC, Manassas VA) that express VCAM-1[9] were grown in Dulbecco's modified Eagle's medium supplemented with 10% fetal bovine serum in culture flasks. For activation, the cells were pre-treated with TNF-α (10 ng/ml) for 2-4 hours. The cells were then removed from the culture flasks by trypsin digestion, centrifuged, and resuspended in cell culture medium. Microbubbles (1×10^6) targeted to murine VCAM-1 were added to suspensions of SVEC4-10 in a total volume of 1 mL and incubated at 37° C for 5 min with intermittent gentle agitation to allow for microbubble attachment to cells. The percentage of microbubbles that were adhered to cells was varied according to the degree of TNF-α-activation and the number of cells added (range of microbubble:cell ratios: 20:1 to 100:1). The relative proportion of free microbubbles and those ligated to endothelial cells was quantified by light microscopy. The microbubble suspensions were diluted 100-fold and loaded into 3 mL dialysis cassettes (Thermo Scientific, Rockford, IL). The cassettes were suspended 3 cm beneath the ultrasound transducer in a water bath (acoustic focus 3 cm). Several frames were first acquired

at an MI of 0.18, after which the MI was increased to 0.97. Videointensity was measured from the upper third of the cassette. Values were averaged from several frames during low MI imaging whereas only the first frame was used from high-MI imaging acquisitions. Pixel intensity histograms were also generated from similar regions-of-interest using raw images before log-linear conversion.

Molecular Imaging of Inflammation in Acute Ischemia

Differences in molecular imaging signal enhancement during low- and high-MI imaging *in vivo* were evaluated in a murine model of acute ischemia-reperfusion injury of the hindlimb. The study was approved by the institutional Animal Care and Use Committee. Imaging was performed in 18 wild-type C57Bl/6 mice and in 6 mice with gene-targeted homozygous deletion of P-Selectin (P-/-). Anesthesia was induced and maintained with inhaled isoflurane. A jugular vein was cannulated for administration of microbubbles. Acute hindlimb ischemia was produced in 12 of the wild-type and all 6 of the P-/- mice by placement of an external occlusion device placed around the proximal hindlimb for 10 minutes. Complete cessation of blood flow in the hindlimb was confirmed by contrast-enhanced ultrasound perfusion imaging during occlusion.

Molecular imaging was performed 45 min after ischemia. The proximal hindlimb adductor muscles were imaged in a transaxial plane leg midway between the inguinal fold and the knee. P-selectin-targeted or control microbubbles (3×10^6 for each) were injected intravenously in random order. After each injection, ultrasound imaging was paused for 10 min after which imaging was resumed at a mechanical index of 0.18. Several frames were acquired, after which the mechanical index was increased to 0.97 with acoustic shielding during power adjustment. The signal from retained targeted agent was derived as previously described.[2] The initial frame at an MI of 0.97 was acquired, after which microbubbles in the sector were destroyed by several more frames. Background images representing freely circulating microbubbles were subsequently acquired at both MI settings with a pulsing interval of 10 s for high MI imaging. The molecular signal was derived by digital subtraction of several averaged post-destruction frames at appropriate MI from several averaged pre-destruction frames for low-MI or the initial frame for high-MI. Regions-of-interest were drawn over the adductor muscle group to measure video intensity for molecular tracer. The raw images were used to generate histograms of pixel videointensity and to analyze the number and percentage of pixels that demonstrated video enhancement (>3 SD beyond mean background signal).

Statistical Methods

Data are expressed as mean values unless otherwise stated. For assessment of microbubble stability when imaged at low MI, a repeated measures ANOVA was used. Correlations were made with Pearson's correlation and least squares fit.

Results

Microbubble Concentration-intensity Relationships

In order to validate comparisons between video intensities, the relation between microbubble concentration and videointensity was performed in an *in vitro* water tank. This relation was relatively linear for both low-MI and high-MI imaging with some slight flattening of the curves at high concentrations which approached dynamic range saturation (Figure 1A). The ratio of signal enhancement at high-MI to that at low-MI (Figure 1B) was approximately 3:1 except at the very lowest microbubble concentrations where signal was extremely low due to the paucity of microbubble events resulting in near-equal background intensity levels.

Acoustic Response from Microbubbles Ligated to Cells

For the *in vitro* cell binding studies, a wide range of attachment efficiency (3% to 31% of all microbubbles) was achieved by combining a constant number of VCAM-1-targeted microbubbles with SVEC4-10 cells in suspension in different concentrations and activation states. Clustering of microbubbles to each other on the cell surface was not observed (Figure 2A), and there was no preferential attachment for microbubbles according to size. At both low-MI and high-MI, the percentage of microbubbles attached did not significantly influence background-subtracted videointensity (Figure 2B), indicating that microbubble ligation to cells did little to alter signal generation at low- or high power in *in vitro* conditions. Despite similar background (pre-contrast) levels, videointensity values were 2-3 fold higher at high-MI compared to low-MI (Figure 2C). High-MI data was only 1.5-1.7 higher than low-MI for similar analysis performed before log-linear conversion of data. Illustrated by the two examples in Figure 3A and 3B, increasing the MI resulted in a rightward shift in the histogram for pixel intensity indicating that high signal enhancement was due, in part, to greater intensity for pixel enhancement.

Power-dependency of Signal Generation During *In vivo* Molecular Imaging

During *in vivo* imaging, there was no decay in signal enhancement for the first 5 frames obtained with low-MI imaging 10 minutes after intravenous injection of P-selectin-targeted microbubbles indicating that destruction was minimal (Figure 4). There was a close linear relationship between the intensity at low-MI and high-MI when all molecular imaging data (control and ischemic limbs, and control and targeted microbubbles) were analyzed (Figure 5). However, as indicated by the slope of the regression line (0.42), signal from microbubbles under any condition was almost 2.5-fold greater for high-MI compared to low-MI imaging. Representative examples of P-selectin imaging in post-ischemic limbs are illustrated in Figure 6A and 6B. The power-related differences between the images and the pixel intensity histograms indicate that increased videointensity for high-power imaging *in vivo* was not due simply to increased pixel intensity. Rather, there was also an increase in the number of pixels or percentage of pixels in a region-of-interest that enhance above background indicating the detection of more microbubbles with high-MI imaging and/or an increase in the point-spread function for microbubble events.

Discussion

The aim of this study was to evaluate the influence of acoustic power on *in vivo* molecular imaging data. Contrast-specific low-MI imaging data was compared with that from high-MI protocols that have been commonly used to detect tissue retention of targeted microbubbles. We demonstrated that high-MI imaging provides more robust signal enhancement than low-MI imaging during *in vivo* molecular imaging. However, the linear relationship between the low-MI and high-MI signal indicates that *relative* differences in signal intensity according to condition or microbubble agent are similar for the two settings, although the *absolute* differences are greater for high-MI imaging.

Justification for this study was based on increasing interest in using low-MI methods for molecular imaging. For example, low-MI imaging of VCAM-1 expression with targeted microbubbles has recently been used to non-invasively evaluate inflammatory phenotype in mouse models of atherosclerosis.[10] In this situation, respiratory motion of the aorta made it necessary to select appropriate frames according to the position of the aorta in the beam elevation and the presence of motion artifact. Selection of optimal frames and frame averaging is possible only with low-MI imaging and multiframe acquisition. Also the ability to optimize the sector location and imaging parameters before acquiring targeted imaging data is possible only with low-MI imaging methods.

In the current study, the issue of microbubble damping during molecular imaging was of particular interest to us since it is possible that ligation of microbubbles to cells may dampen their vibration and their ability to produce non-linear oscillation at low acoustic pressures.[7,8] The nonlinear oscillation of microbubbles is predicted by the Rayleigh-Plesset equation and modifications thereof indicate that damping from boundary conditions can affect microbubble behavior in an ultrasound field.[4-6] This effect serves to explain the reduction in the acoustic lability and signal generation for microbubbles in the extreme situation when microbubbles have been phagocytosed by granulocytes and are influenced by the intracellular milieu.[3,11] Traditional models do not necessarily account for the asymmetric forces on a bubble created by external ligation to a cell. To study this issue, we did not measure acoustic amplitude directly but rather took a more pragmatic approach which was to measure intensity provided by a clinical imaging system. The *in vitro* imaging experiments with cell-microbubble suspensions were carried out to prove that damping from microbubble attachment at either high-MI or low-MI was insufficient to influence videointensity, at least in the ranges of attachment percentage achieved in this study. If damping or loss of signal generation occurred from attachment, then we should have seen a significant negative slope in the curves defining the relation between percent attachment and intensity. Instead the regression lines were flat. The degree of damping is influenced by the material properties of the substance to which microbubbles are attached.[8] Hence, the lack of influence of attachment on signal intensity may be secondary to the ability of microbubble oscillation to easily displace adjacent endothelial cell membranes which has been observed by high-speed video microscopy.[12]

During *in vitro* imaging, videointensity was 2-3-fold greater for high-MI versus low-MI imaging despite having similar gain-compensated background intensities. Similarly, during *in vivo* molecular imaging where signal intensity was varied by the presence/absence of limb ischemia and microbubble type, high-MI imaging provided a 2-2.5-fold increase in intensity. It is worth noting that the ratio of high-MI to low-MI signal was substantially affected by the log-linear conversion. Signal during high-MI imaging was only 50-70% greater when videointensity was measured from log-compressed digital data from the ultrasound system. Greater intensity for high-MI imaging *in vivo* was not simply due to increased pixel intensity. There were also a greater number of pixels that enhanced at the high-MI setting. Visual inspection of the images indicated that the greater spatial extent of enhancement was due to a greater point-spread function creating a halo effect around regions with intense enhancement, as well as appearance of microbubble events that were not seen by low-MI imaging.

Although high-MI imaging provided more robust enhancement, molecular signal at low and high power correlated linearly. This finding indicates that the power settings would not substantially affect the relative change in signal enhancement or relative difference between animals, tissue or contrast agents.

There are several limitations of the study that deserve mention. As mentioned previously, the rather large differences in low-MI and high-MI intensity reflect the log-linear conversion which we believed to be necessary to compare wide ranges of intensity values. Also, these studies were performed at relatively high ultrasound frequency in a small animal model of disease where there was little attenuation from body structures. However, previous *in vitro* studies with lower acoustic frequencies have indicated that cell attachment produces only a mild degree of signal damping.[8] The high imaging frequency raises a second unresolved issue. Since resonant frequency for a microbubble is influence by the shell viscoelastic properties,[4,5] it is possible that microbubble ligation to cells may have increased its resonant frequency closer to 7 MHz range used in this study, which may have minimized the affects of attachment-related damping. We also did not perform a comprehensive test of all possible power and frequency combinations. Instead, we chose to focus our efforts on power settings that are conventionally used for multipulse contrast-specific imaging algorithms. We also did not perform

radiofrequency analysis from microbubbles. Finally, data from in vitro studies would have been more robust if free microbubbles were eliminated. This was not done because of inability to use electrozone counting after ligation to correct for concentration.

In summary, we have found that low-MI molecular imaging with a multipulse contrast-specific imaging method is feasible and provides similar information as high-MI imaging in terms of relative contrast enhancement. Damping does not appear to be a major constraint to low-MI imaging. However, more robust contrast enhancement can be expected when using high-MI imaging methods for detecting targeted microbubble retention in tissue. The choice of power settings for molecular imaging protocols should therefore be made according to a balance of considerations such as sensitivity, likelihood for artifacts, ease of use, and need to acquire different imaging planes.

Acknowledgments

Supported by grants (R01-DK063508, R01-HL078610, and R01-HL074443) to Dr. Lindner from the National Institutes of Health, Bethesda, Maryland. Dr. Kaufmann is supported by a research grant from the Lichtenstein Foundation; and Dr. Carr is supported by a Post-doctoral Fellowship Grant from the American Heart Association.

References

1. Kaufmann B, Wei K, Lindner JR. Molecular Imaging with Targeted Contrast Ultrasound. Curr Opin Biotech 2007;18:11–16. [PubMed: 17241779]
2. Lindner JR, Song J, Christiansen J, Klibanov AL, Xu F, Ley K. Ultrasound assessment of inflammation and renal tissue injury with microbubbles targeted to P-selectin. Circulation 2001;104:2107–12. [PubMed: 11673354]
3. Lindner JR, Song J, Xu F, Klibanov AL, Singbartl K, Ley K, et al. Noninvasive ultrasound imaging of inflammation using microbubbles targeted to activated leukocytes. Circulation 2000;102:2745–50. 28. [PubMed: 11094042]
4. Church CC. The effects of an elastic solid surface layer on the radial pulsations of gas bubbles. J Acoust Soc Am 1995;97:1510.
5. Khismatullin DB, Nadim A. Radial oscillations of encapsulated microbubbles in viscoelastic liquids. Phys Fluids 2002;14:3534–3557.
6. de Jong N, Hoff L, Skotland T, Bom N. Absorption and scatter of encapsulated gas filled microspheres: theoretical considerations and some measurements. Ultrasonics 1992;30:95–103. [PubMed: 1557838]
7. Zhao S, Kruse DE, Ferrara KW, Dayton PA. Acoustic response from adherent targeted contrast agents. J Acoust Soc Am 2006;120:EL63–EL69. [PubMed: 17225437]
8. Lankford M, Behm CZ, Yeh J, Klibanov AL, Robinson P, Lindner JR. Effect of microbubble ligation to cells on ultrasound signal enhancement: implications for targeted imaging. Invest Radiol 2006;41:721–8. [PubMed: 16971795]
9. Sasaki M, Ostanin D, Elrod JW, Oshima T, Jordan P, Itoh M, et al. TNF-alpha - induced endothelial cell adhesion molecule expression is cytochrome P-450 monooxygenase dependent. Am J Physiol Cell Physiol 2003;284:C422–C428. [PubMed: 12388057]
10. Kaufmann BA, Sanders JM, Davis C, Xie A, Aldred P, Sarembock IJ, et al. Molecular imaging of inflammation in atherosclerosis with targeted ultrasound detection of vascular cell adhesion molecule-1. Circulation 2007;116:276–84. [PubMed: 17592078]
11. Dayton PA, Chomas JE, Lum A, Allen J, Lindner JR, Simon SI. Optical and acoustical dynamics of microbubble contrast agents inside neutrophils. Biophys J 2001;80:1547–1556. [PubMed: 11222315]
12. van Wamel A, Bouakaz A, Versluis M, de Jong N. Micromanipulation of endothelial cells: ultrasound-microububble-cell interaction. Ultrasound Med Biol 2004;30:1255–1258. [PubMed: 15550330]

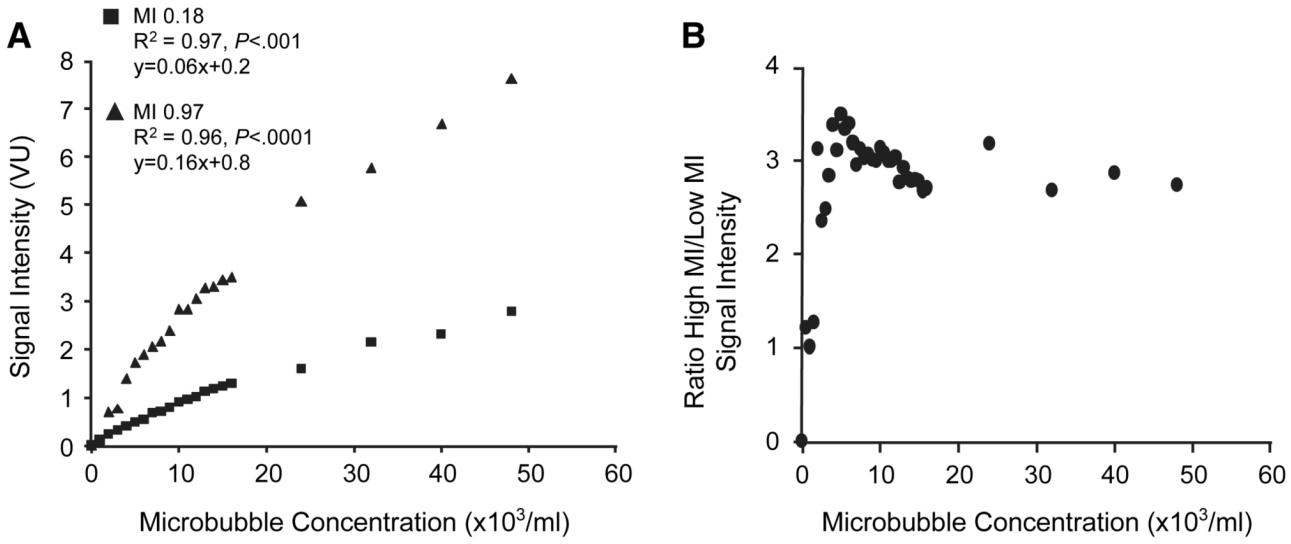

Figure 1.

Imaging data from i*n vitro* water tank experiments after log-linear transformation. (**A**) Relation between microbubble concentration signal enhancement at low- and high-MI. VU, videointensity units. (**B**) Ratio of high-MI to low-MI signal enhancement over the range of microbubble concentrations studied.

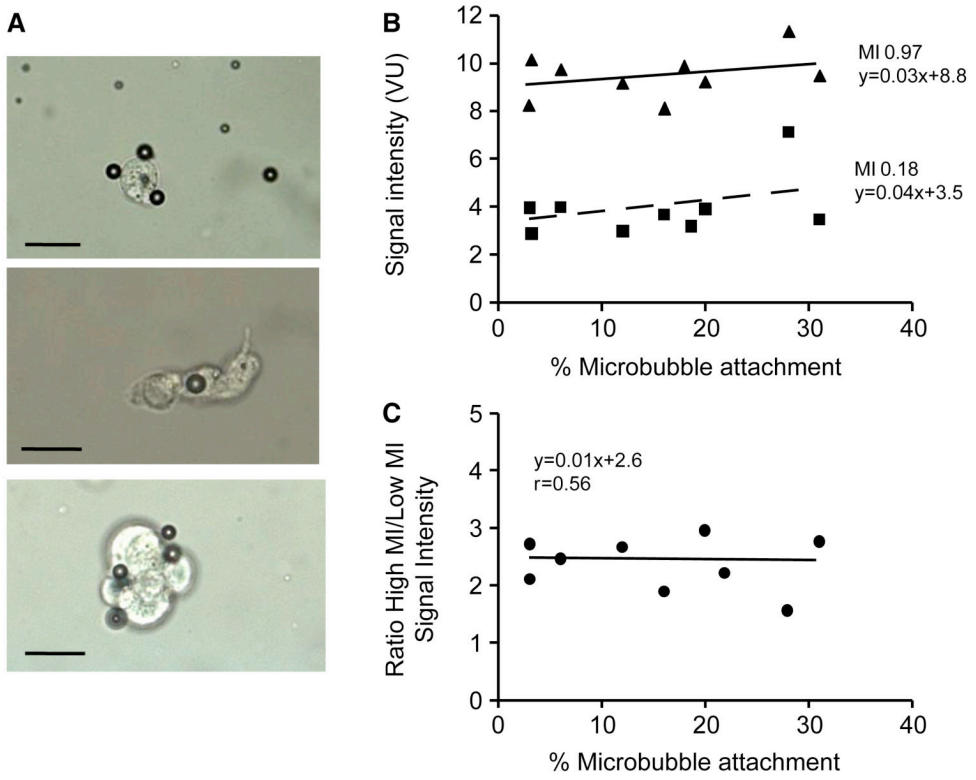

Figure 2.

Influence of microbubble-cell attachment on signal generation in an *in vitro* phantom. (**A**) Examples of VCAM-1-targeted microbubbles attaching to TNF-α-activated SVEC4-10 cells by light microscopy. Scale bar = 20 μm. (**B**) Relation between the percentage of VCAM-1-targeted microbubbles attached to SVEC4-10 cells and background-subtracted signal enhancement during low-MI and high-MI imaging. The slopes are not significantly different from zero (p=0.24 and p=0.46 for high and low MI, respectively) (**C**) Ratio of high-MI to low-MI signal enhancement according to the extent of microbubble attachment to SVEC4-10 cells.

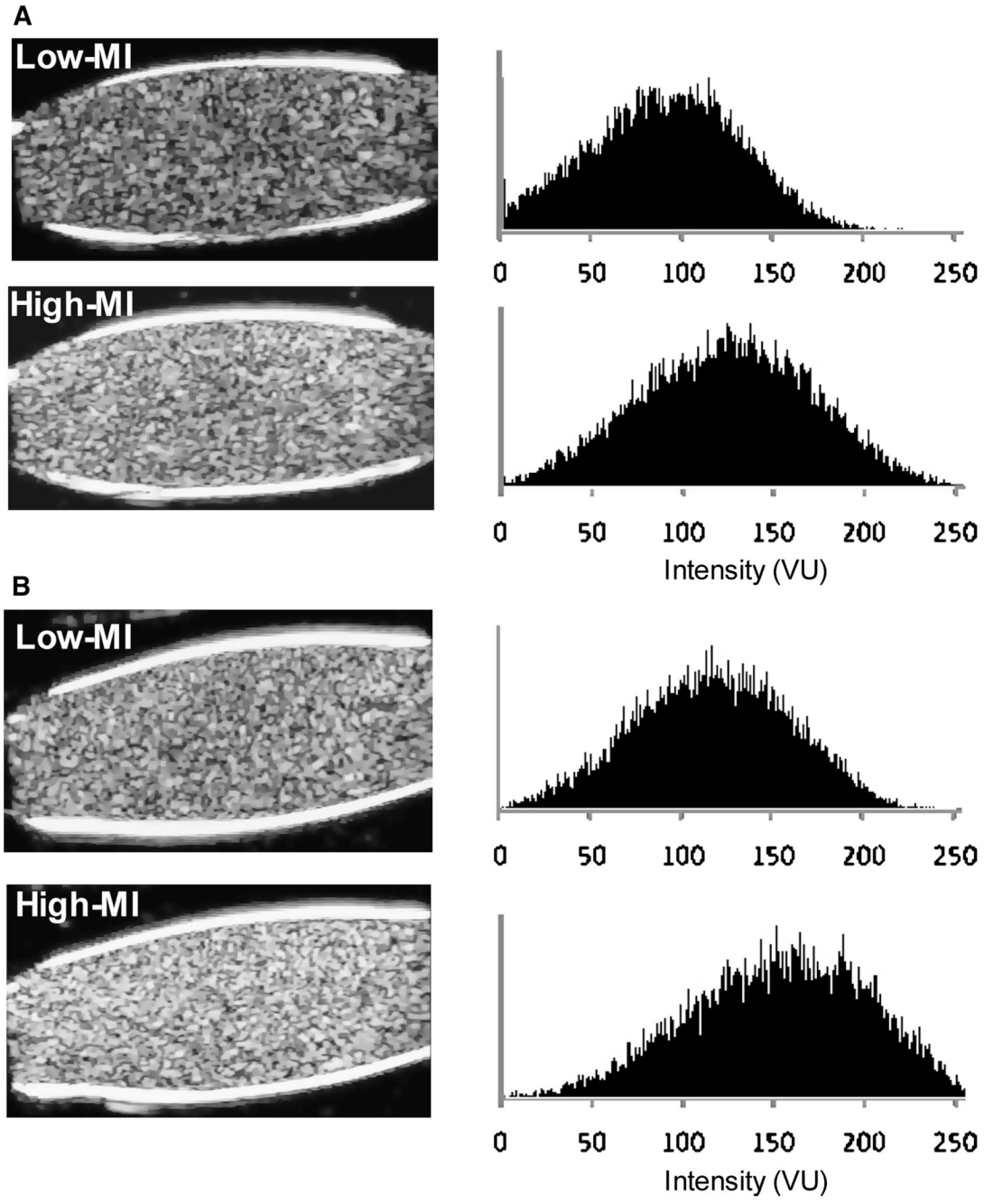

Figure 3.
Two examples (**A** and **B**) of log-compressed images of *in vitro* microbubble-cell suspensions imaged at low-MI and high-MI settings, and corresponding histograms of pixel intensity on a 256 gray-scale range. VU, videointensity units.

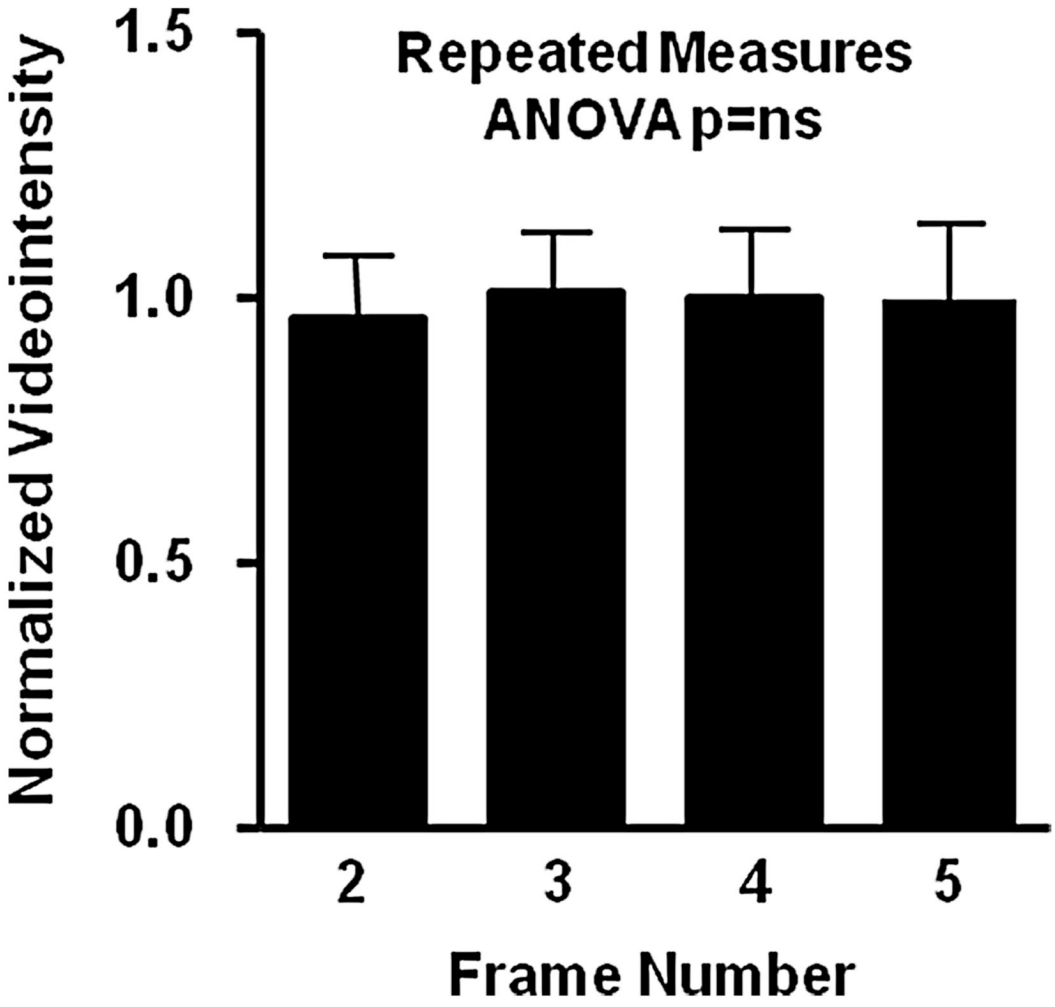

Figure 4.

Background-subtracted intensity of the 2nd to 5th frame normalized to the initial frame from low-*in vivo* targeted molecular imaging of P-selectin in post-ischemic hindlimb muscle. These data indicate that the settings used for low-MI imaging were appropriate and did not gradually destroy microbubbles

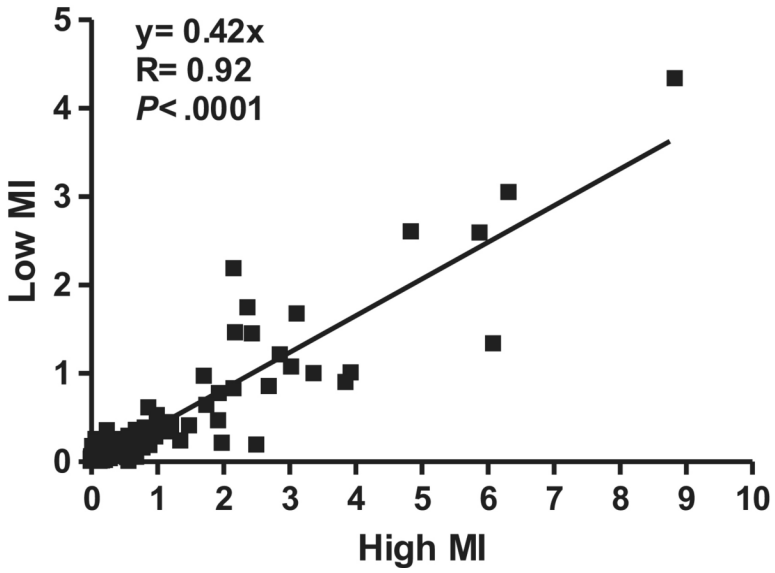

Figure 5.
Relation between high-MI and low-MI background subtracted videointensity during *in vivo* molecular in a murine model of hindlimb ischemia-reperfusion injury.

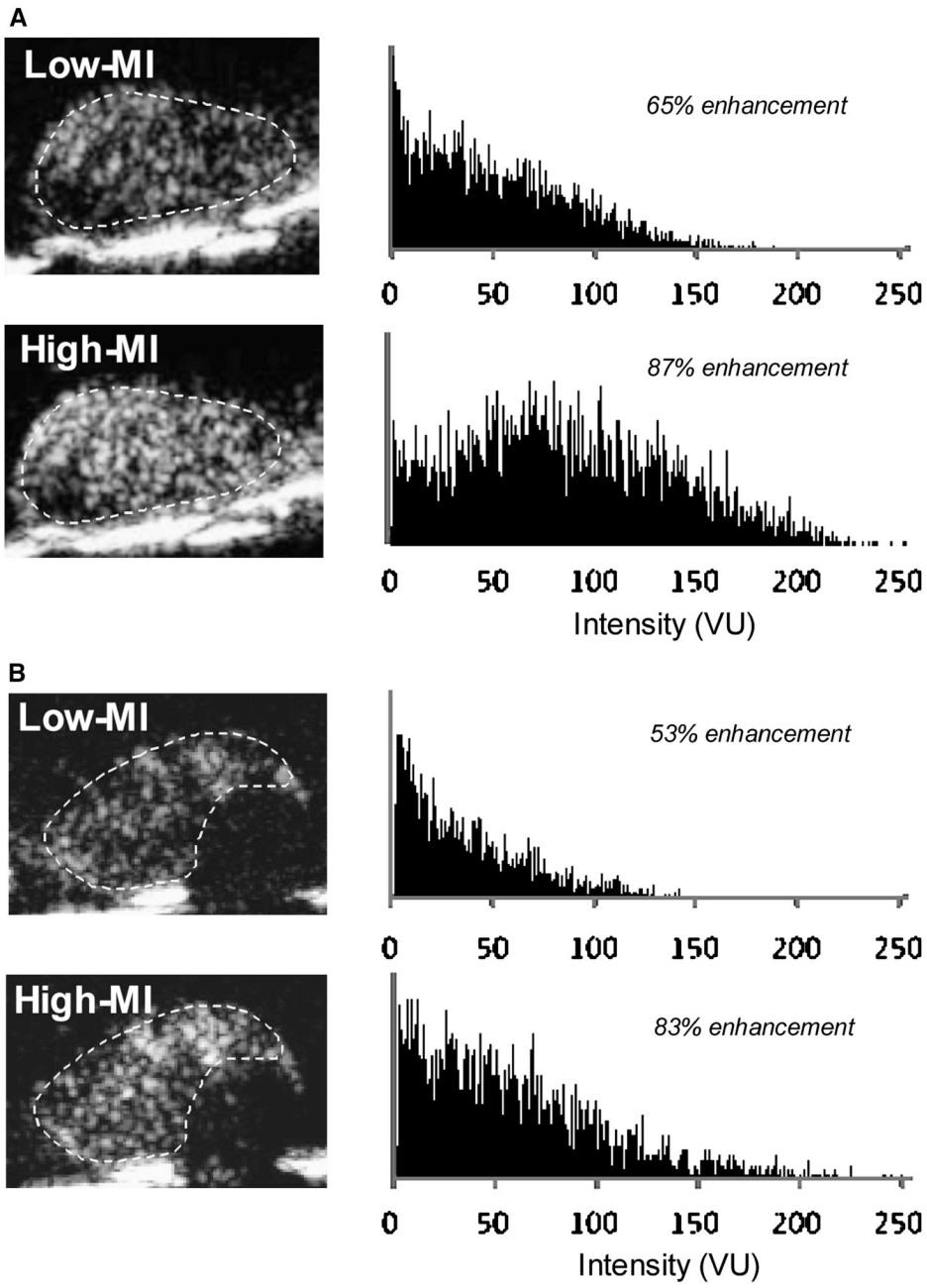

Figure 6.

Representative examples from two separate animals (**A** and **B**) of log-compressed images obtained with P-selectin-targeted microbubbles imaged at low-MI and high-MI settings, and corresponding histograms of pixel intensity on a 256 gray-scale range from a region-of-interest (dashed line) placed around the adductor muscle group. The percent enhancement values represent the fraction of pixels within the region-of-interest that demonstrate enhancement according to the pixel intensity threshold analysis. VU, videointensity units.